Front. Phys. 10, 103101 (2015)
DOI 10.1007/s11467-014-0430-4

RESEARCH ARTICLE

Secondary plasmon resonance in graphene nanostructures

Yang Li[1], **Hong Zhang**[1,2,†], **Da-Wei Yan**[3], **Hai-Feng Yin**[4], **Xin-Lu Cheng**[2]

[1] *College of Physical Science and Technology, Sichuan University, Chengdu 610065, China*

[2] *Key Laboratory of High Energy Density Physics and Technology of Ministry of Education, Sichuan University, Chengdu 610065, China*

[3] *Research Center of Laser Fusion, China Academy of Engineering Physics, Mianyang 621900, China*

[4] *College of Science, Kaili University, Kaili 556011, China*

Corresponding author. E-mail: [†] *hongzhang@scu.edu.cn*

Received April 14, 2014; accepted June 5, 2014

The plasmon characteristics of two graphene nanostructures are studied using time-dependent density functional theory (TDDFT). The absorption spectrum has two main bands, which result from π and $\sigma + \pi$ plasmon resonances. At low energies, the Fourier transform of the induced charge density maps exhibits anomalous behavior, with a π phase change in the charge density maps in the plane of the graphene and those in the plane 0.3 Å from the graphene. The charge density fluctuations close to the plane of the graphene are much smaller than those above and beneath the graphene plane. However, this phenomenon disappears at higher energies. By analyzing the electronic properties, we may conclude that the restoring force for the plasmon in the plane of the graphene does not result from fixed positive ions, but rather the Coulomb interactions with the plasmonic oscillations away from the plane of the graphene, which extend in the surface-normal direction. The collective oscillation in the graphene plane results in a forced vibration. Accordingly, the low-energy plasmon in the graphene can be split into two components: a normal component, which corresponds to direct feedback of the external perturbation, and a secondary component, which corresponds to feedback of the Coulombic interaction with the normal component.

Keywords time-dependent density functional theory (TDDFT), graphene nanostructure, plasmon, induced charge

PACS numbers 31.70.Hq, 32.80.Wr

Frontiers of Physics

1 Introduction

Collective electronic oscillations in metals or semiconductors lead to surface plasmon resonance, which enables confinement and control of electromagnetic energy at sub wavelength length scales [1–5]. Plasmons in nanostructures can be tuned by modulating the shape or size of the structure [6, 7], and so materials of this kind have great potential for applications in sensing, spectroscopy [8, 9], catalytic reactions [10] and biomedical treatments [11]. Benefitting from advances in the fabrication of nanodevices that enable preparation of samples with excellent control over the size and shape [2, 12, 13], plasmonics is a field that has experienced recent rapid growth. However, the quest for new nanostructures with novel functionality represents a major ongoing effort in nanoplasmonics and condensed matter physics [14–16].

Since the discovery of graphene, it has attracted considerable research interest mainly due to the peculiar electronic properties. It is a two-dimensional material and exhibits band structure that features so-called Dirac points and Dirac cones. At the Dirac point, the vertices of the valence bands and the conduction bands meet at the Fermi energy. Because of the zero density of states at the Dirac point, the electronic conductivity is quite low; however, at elevated temperatures, if doped with suitable elements or with an appropriate bias voltage, the conductivity can be increased [17]. Furthermore, the electronic mobility of graphene is very large, and the electrons in graphene exhibit ballistic transport [17–20]. The physical properties described above make graphene a particularly promising material for carbon-based electronics. Because of the ballistic transport, charge carriers may propagate for long distances, making graphene a potential material to substitute for noble metals used to fabricate plasmonics devices, without incurring the large optical losses of surface plasmons [21–23].

In recent years, plasmonics with graphene nanostructures has attracted growing attention. Wang *et al.* [24] studied graphene edge plasmons in finite graphene nanostructures. For a linear edge profile, graphene supports fewer edge modes than a two-dimensional electron gas (2DEG) with a given wave vector q, and the edge monopole plasmon dispersion in graphene follows a $q^{1/4}$ law in contrast to the q^0 law observed for 2DEGs. Recently, the collective excitation of graphene nanostructures with hexagonal and rectangular geometries has been studied [7]. Based on these calculations, the authors reported some interesting observations: the edge configuration is significant in the optical absorption spectrum of graphene nanostructures, and the width of the graphene nanostructure also influences the optical absorption spectrum. Real-space images of the plasmon fields can be acquired directly using a scattering-type scanning near-field optical microscope (SNOM) [25, 26]. A SNOM uses metal AFM tips as near-field probes. When the tips are illuminated using infrared laser light, they act as optical antennas that convert the incident light into a localized near field below the tip apex. The localized near field then lunches plasmons that are reflected at the edges, and form standing waves. The standing waves can be imaged from the light that is scattered by the tips using a pseudo-heterodyne interferometer.

The collective excitation of electrons can be described using time-dependent density functional theory (TDDFT) [1, 7, 27–31]. Surface plasmon excitations of C_{60} clusters have been calculated using a spherically averaged pseudo potential model combined with the density functional formalism for the ground state, and TDDFT for the response function [27], and the properties of the collective excitations of the C_{60} cluster were described. Yan *et al.* [28] investigated the collective excitation of electrons in linear chains of atoms and predicted the existence and nature of the end and central plasmon resonances in the chains.

In this work, we examine the motion of the electrons when plasmons are excited in graphene nanostructures. Two graphene nanostructures are employed in our work: a triangular structure and a rectangular structure. The plasmons are excited in the graphene plane. To characterize the motion of electrons, we display a set of frequency-dependent density maps of different layers. We define P_x as the plane that parallel to plane of the graphene but separated by a distance x. We find that in each low-energy resonance point, the Fourier transform of the induced charge density maps exhibits an anomalous behavior, with a π phase change in the charge density maps in the plane of the graphene and those in the plane 0.3 Å from the graphene. In addition, we carried out calculations for a 7×7 array of Na atoms for comparison.

2 Optical absorption spectra from time-dependent density-functional theory

TDDFT is a quantum mechanical theory used in physics and chemistry to investigate the electronic properties and dynamics of many-body systems in the presence of time-dependent potentials. The collective oscillations of electrons in the graphene nanostructures are time-dependent; therefore, TDDFT is an ideal tool for our study. In our calculations, we propagate the time-dependent Kohn–Sham equations in real time to obtain optical absorption spectra [32]. Because we will obtain a similar result was reported by Yan [28], who used the method developed by Casida, we calculate the linear response of the electrons to an external potential in the frequency domain [33]. Before $t = 0$, the system was assumed to lie in the ground state. It then experiences an instantaneous perturbation described by the following potential [34]

$$v(r,t) = -\hbar k_0 x_\nu \delta(t), \tag{1}$$

where $x_\nu = x, y, z$ denotes the polarization direction and k_0 is the momentum transferred to the system. To ensure that the response of the system in response to the perturbation was linear, the perturbation should to be small. However, it should also be sufficiently large that we avoid the response being lost in noise. By applying a suitable an external field, all frequencies of the system can be excited equally. We define $\varphi_i(r)$ as the ground-state Kohn–Sham wavefunction of the system, and the initial state for time evolution at $t = 0^+$ can be expressed as [34]

$$\psi_i(r,0^+) = \exp(\mathrm{i}k_0 x_v)\varphi_i(r). \tag{2}$$

The Kohn–Sham wavefunctions are then propagated for a finite time. Information on the excitation can then be deduced from the dipole-strength function $S(\omega)S(\omega)$, which measures how strongly a given frequency ω excites the system and it can be expressed as [32, 34]

$$S(\omega) = \frac{2m_e\omega}{\pi\hbar e^2}\Im\sum_v \alpha_{vv}(\omega), \tag{3}$$

where the dynamic polarizability $a_{\mu v}(\omega)$ is given by

$$\alpha_{\mu\nu} = \frac{e^2}{\hbar k_0}\int \mathrm{d}r x_v \delta n(r,\omega). \tag{4}$$

3 Computational details

The calculations were implemented using real-space and real-time TDDFT simulations using the software package Octopus [35]. The carbon, hydrogen and sodium atoms were described using Troullier–Martins pseudo potentials [36]. The local density approximation (LDA) for the exchange correlation was used in both the ground state and excited state calculations as described by Marinopoulos *et al.* [37]. The three simulation zones were cuboids, where the bottom faces were square. The lengths of the sides were 24 Å, 28 Å for the triangular and rectangular graphene nanostructures, respectively, and were and 28 Å for the Na array. The corresponding heights of the cuboids were 15 Å, 16 Å and 15 Å. The space was discredited into uniform grids, and the interval between adjacent grids was 0.3 Å. The length, the width and the height of the cuboids were parallel to the X, Y and Z axes, respectively. The graphene nanostructure and the Na array were located at the center of the cuboids, which also formed the origin of the coordinate system. In the plane-wave propagation, excitation spectra were extracted via Fourier transforming the dipole strength induced by the impulse excitation. During the real-time propagation, the electronic wave packets were evolved for typically 6000 steps, where each time step was 0.005 $\hbar$/eV. To study the motion of the electrons, we acquired the induced charge density of each grid, where the induced charge density is the difference between the charge density at time t and time 0, i.e., $\boldsymbol{\rho}(\boldsymbol{r},t)-\boldsymbol{\rho}(\boldsymbol{r},0)$. The Fourier transform was used to transform the induced charge density from time domain into frequency domain; i.e.,

$$\Delta\rho(r,\omega)=\frac{1}{T}\int_0^T[\rho(r,t)-\rho(r,0)]\mathrm{e}^{-\mathrm{i}\omega t}\mathrm{d}t. \tag{5}$$

where $\rho(r,0)$ and $\rho(r,t)$ are the charge density at time 0 and t and spatial coordinate $\boldsymbol{r}$. Here $\Delta\rho(r,\omega)$ represents the population of electrons that oscillate with frequency $\boldsymbol{\omega}$ at point $\boldsymbol{r}$. It corresponds to a plasmon oscillation of a given frequency.

The graphene nanostructures were passivated by hydrogen atoms at the edges. The interval between two adjacent Na atoms was 2.89 Å [28, 38]. To simplify the problem, the atoms were fixed and only changes in electrons were taken into consideration in our calculations. First, we discuss the electronic oscillations in the triangular graphene. We then discuss the corresponding results from the rectangular graphene. Finally, the oscillations in the 7×7 Na array are discussed for comparison.

4 Results and discussion

Figure 1 shows the dipole response (i.e., optical absorption) of the triangular nanostructure in response to impulse excitations polarized in the X and Y directions. Because the external perturbation was a vector of electric field, the perturbation in any direction of the graphene plane can be decomposed into X and Y components. These results can be understood by considering that there are two main surface plasmon bands when excited from any direction of the graphene plane. That with an energy of approximately 16 eV is termed the $\sigma+\pi$ plasmon resonance, and that with an energy of approximately 5 eV is termed the π plasmon resonance. Because of the ballistic transport property of graphene, the collective oscillations of the low-energy zone are not significantly affected by the various C atoms at the interior of the structure, and only those near the boundaries are significant. In our simulations, the graphene nanostructures were terminated by zigzag edges. Therefore, when excited in the X and Y directions, they had almost identical absorption spectra at low energies. This conclusion applies to any excitation direction of the graphene nanostructure.

To obtain further details of these plasmons, we analyzed the Fourier transform of induced time-dependent charge density. Figure 2 shows charge density maps of some low-energy resonances. Comparing the first and second columns of images shown in Fig. 2, we find that for each high-density region in P_0, there is a zone with the opposite density distribution at $P_{0.3}$. It follows that, in this plasmon mode, the electrons in the two zones oscillate in opposite directions. This is an interesting observation that has not been reported previously. To observe this more clearly, we consider the snapshot across the X axis shown in Fig. 3. It makes sure that the high density region close to P_0 only occupies a very small volume with respect to that in the surface normal direction. Figure 4 shows charge density maps of the resonance point at 16.6 eV. The distributions in P_0 and $P_{0.3}$ appear almost

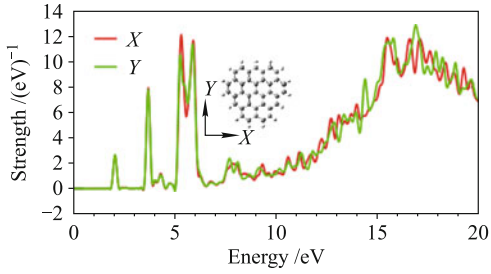

Fig. 1 The dipole response (optical absorption) of the triangular graphene nanostructure in response to impulse excitations polarized in the X and Y directions.

identical, and the opposing phase of different regions of charge density seen with the lower-energy mode was not observed for this higher-energy resonance.

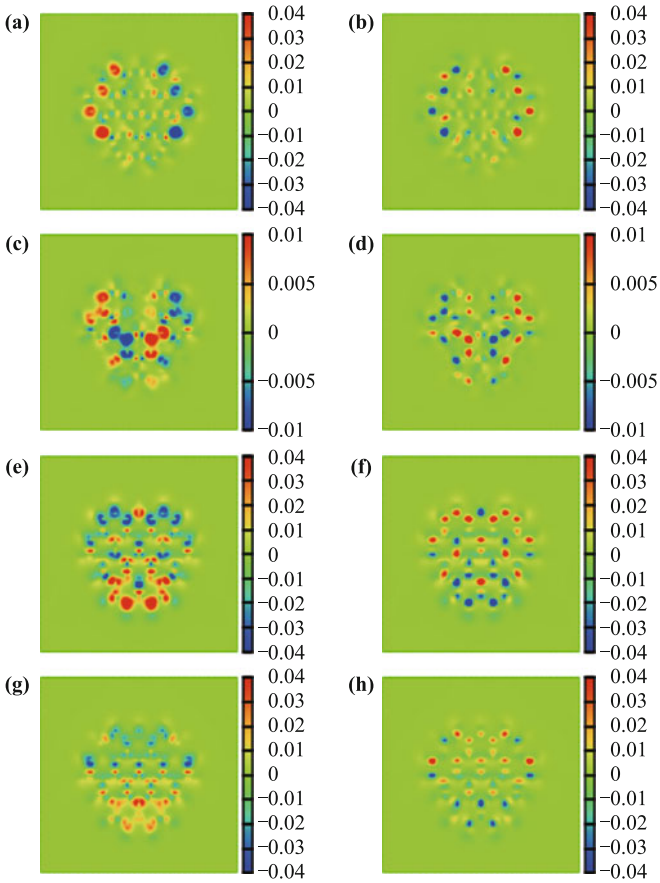

Fig. 2 The Fourier transform of induced charge density for the triangular structure. The first column shows P_0 and the second shows $P_{0.3}$. **(a)** and **(b)** Excitation from the Xdirection and at the resonance at 2.04 eV. **(c)** and **(d)** Excitation from the X direction at the resonance at 4.29 eV. **(e)** and **(f)** Excited from the Y direction at 3.68 eV. **(g)** and **(h)** Excitation from the Y direction at 5.87 eV.

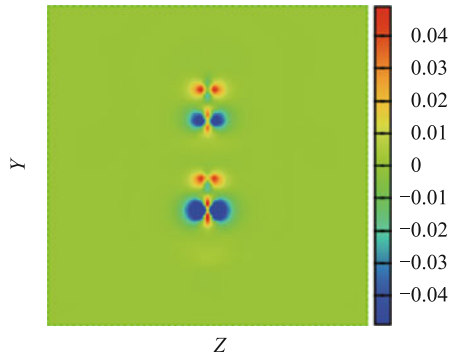

Fig. 3 Fourier transform of the induced charge density for the triangular structure in the plane $x = -3.6$ Å when excited from X direction at 2.04 eV.

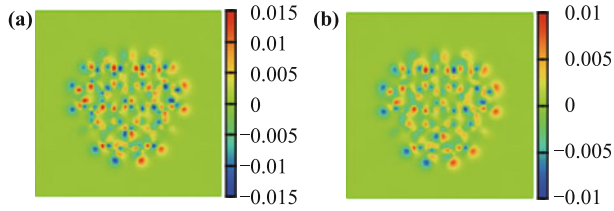

Fig. 4 The Fourier transform of induced charge density for the triangular structure at 16.6 eV when excited from X direction. **(a)** at P_0 and **(b)** at $P_{0.3}$.

We have discussed the plasmonic properties of the rectangular structure shown in Fig. 5 previously [7]. The data reported in Ref. [7], include spectra revealing two bands, which were similar to those shown in Fig. 1; however, the two spectral lines differed significantly at low energies. This is because of the different edge conditions in the X and Y directions.

Figure 6 shows charge density maps of the rectangular nanostructure at selected low-energy resonances. Compared with the data shown for the triangular structures (see Fig. 2), we obtain the same phenomena in terms of the opposing phase of the oscillations at P_0 and $P_{0.3}$.

To explain data plotted in Figs. 2 and 6, we analyze the binding characteristics of the graphene nanostructures. In the ground state of the C atom, the configuration of the valence electrons is $2s^2 2p^2$. When graphene forms, the configuration becomes to $2(sp^2)^3 2p$. The p electrons of adjacent C atoms overlap and form π–π bonds, which are weak. The delocalized π electrons tend to spread above and below the plane of the graphene, and are π asily excited by external electric field, and

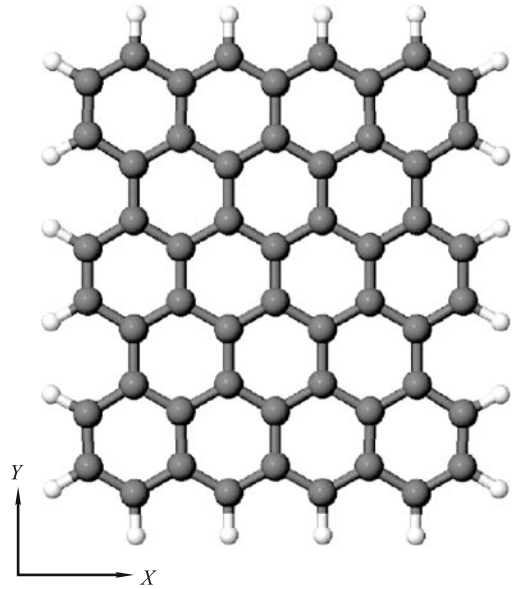

Fig. 5 A schematic diagram showing the rectangular graphene nanostructure.

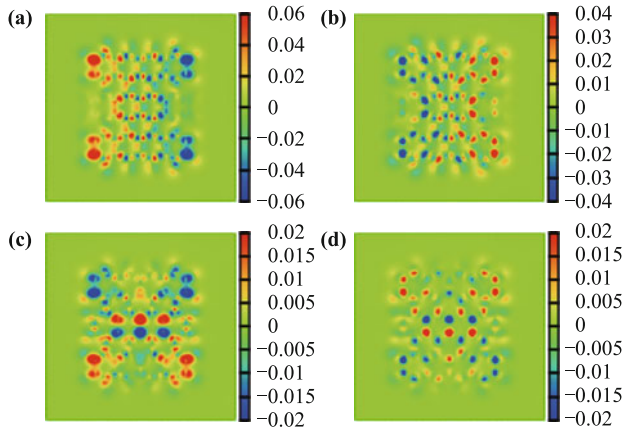

Fig. 6 Fourier transforms of induced charge density for the triangular structure. The first column shows P_0 and the second shows $P_{0.3}$. **(a)** and **(b)** Excitation from the X direction and at the resonance at 2.04 eV. **(c)** and **(d)** Excitation from the X direction at the resonance at 5.08 eV. **(e)** and **(f)** Excitation from the Y direction at the resonance at 5.24 eV.

contribute to both the low-energy and high-energy plasmons. The sp^2 electrons overlap with the $2sp^2$ orbitals of adjacent C atoms (or H atoms in the edge regions), and form in-plane σ bonds, which are stronger than the π–$\pi\pi$ bonds. The σ electrons are located close to P_0, and are σ ifficult to excite, and so only contribute to the higher-energy plasmons.

At low energies, the electrons in σ bonds do not respond to the in-plane perturbation directly. The density distribution at P_0 does not correspond to the response of electrons in σ bonds to external perturbations, rather to the oscillations due to the change in the charge density distribution of π electrons. The oscillations formed by π electrons will exert Coulombic forces on the electrons at P_0, which causes them to oscillate in the opposite direction; i.e., the oscillations at P_0 are forced vibrations, and this leads to the opposing phase of the charge density oscillations at in the planes P_0 and $P_{0.3}$. Because the σ electrons at P_0 are tightly bound, the Coulombic forces may only result in small movements of the σ electrons. This is why the charge density oscillations at P_0 are relatively localized (see Fig. 3). The low-energy plasmons can be divided into two components: normal components located above and beneath the plane of the graphene, and secondary components located close to the plane of the graphene. With the high-energy plasmon modes, both the σ and π valence electrons are involved, and there is no obvious difference in the charge density oscillations at P_0 and $P_x(|x| > 0)$.

To provide a comparison, we also calculate the charge density oscillations in a 7×7 array of Na atoms excited in the X direction. The absorption spectrum exhibited a main peak at 1.92 eV. Figure 7 shows charge density maps at different at this resonance. The three charge density maps appear almost identical. The reason for this is that all the valence electrons consist of 3s orbitals, which are able to respond to the external perturbation directly. The behavior is similar to the high-energy plasmon modes in the graphene nanostructure. Many metal-based plasmonic devices exhibit similar behavior to the Na array, and the charge density maps in different planes do not exhibit the anomalous phase behavior that was observed for the graphene nanostructures.

5 Conclusions

We have investigated the collective excitation of two graphene nanostructures and an array of Na atoms using time-dependent density functional theory (TDDFT). At low energies, the edges of the graphene nanostructures are significant in the optical absorption spectra because of the nature of ballistic charge transport. The low-energy plasmon modes in the graphene nanostructures differ significantly from those of metals, and can be divided into a normal component and a secondary component. The former is located above and beneath the graphene plane, and responds directly to the external perturbation. The latter is located closer to the plane of the graphene, is generated by Coulombic interactions with the charge density fluctuations of the normal component; furthermore, the spatial extent of the secondary

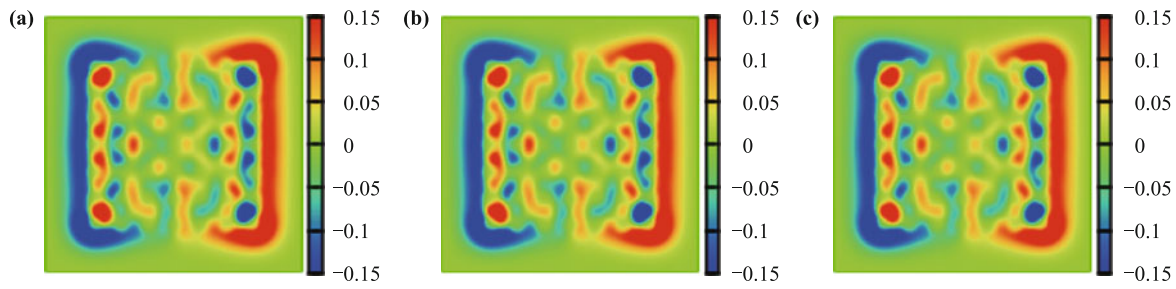

Fig. 7 Fourier transforms of the induced charge density for the 7×7 array of Na atoms at the resonance at 1.92 eV. **(a)** The charge density at P_0, **(b)** at $P_{0.3}$ and **(c)** at $P_{0.6}$ when excited from the X direction.

component is significantly smaller than that of the normal component. Both oscillate in the same direction but with a phase difference of π. The secondary plasmon mode disappears at higher energies because the σ valence electrons are able to respond directly to the external perturbation. Although only two graphene nanostructures were studied, we expect that this phenomenon will be observed in many other graphene structures.

Using a SNOM, it is possible to image and the normal plasmons in graphene; however, the secondary plasmons described here involve charge density fluctuations over very small length scales close to the plane of the graphene. However, it may be feasible to capture the photons emitted by the normal plasmons and the secondary plasmons. At resonance, if a sufficiently strong excitation signal is used, and a weak signal with a phase difference of π can be obtained, this will support the existence of the secondary plasmons described here.

Acknowledgements We would like to acknowledge financial support from the National Natural Science Foundation of China (Grant No. 11074176) and the support from Research Fund for the Doctoral Program of Higher Education of China (Grant No. 20100181110080).

References

1. A. H. Atwater, The promise of plasmonics, *Sci. Am.* 296(4), 56 (2007)
2. J. A. Schuller, E. S. Barnard, W. Cai, Y. C. Jun, J. S. White, and M. L. Brongersma, Plasmonics for extreme light concentration and manipulation, *Nat. Mater.* 9(3), 193 (2010)
3. P. R. West, S. Ishii, G. V. Naik, N. K. Emani, V. M. Shalaev, and A. Boltasseva, Searching for better plasmonic materials, *Laser & Photonics Reviews* 4(6), 795 (2010)
4. M. I. Stockman, Nanoplasmonics: The physics behind the applications, *Phys. Today* 64(2), 39 (2011)
5. L. M. Tong and H. X. Xu, Frontiers of plasmonics, *Front. Phys.* 9(1), 1 (2014)
6. N. Nayyar, A. Kabir, V. Turkowski, and T. S. Rahman, Transition metal impurity-induced generation of plasmonic collective modes in small gold clusters, arXiv: 1109.0905v1 (2011)
7. H. F. Yin and H. Zhang, Plasmons in graphene nanostructures, *J. Appl. Phys.* 111(10), 103502 (2012)
8. S. M. Nie and S. R. Emery, Probing single molecules and single nanoparticles by surface-enhanced Raman scattering, *Science* 275(5303), 1102 (1997)
9. H. X. Xu, E. J. Bjerneld, M. Kall, and L. Borjesson, Spectroscopy of single hemoglobin molecules by surface enhanced Raman scattering, *Phys. Rev. Lett.* 83(21), 4357 (1999)
10. A. T. Bell, The impact of nanoscience on heterogeneous catalysis, *Science* 299(5613), 1688 (2003)
11. L. R. Hirsch, R. J. Stafford, J. A. Bankson, S. R. Sershen, B. Rivera, R. E. Price, J. D. Hazle, N. J. Halas, and J. L. West, Nanoshell-mediated near-infrared thermal therapy of tumors under magnetic resonance guidance, *Proc. Natl. Acad. Sci. USA* 100(23), 13549 (2003)
12. S. Lal, S. Link, and N. J. Halas, Nano-optics from sensing to waveguiding, *Nat. Photonics* 1(11), 641 (2007)
13. P. Nagpal, N. C. Lindquist, S. H. Oh, and D. J. Norris, Ultrasmooth patterned metals for plasmonics and metamaterials, *Science* 325(5940), 594 (2009)
14. W. L. Barnes, A. Dereux, and T. W. Ebbesen, Surface plasmon subwavelength optics, *Nature* 424(6950), 824 (2003)
15. K. L. Kelly, E. Coronado, L. L. Zhao, and G. C. Schatz, The optical properties of metal nanoparticles: The influence of size, shape, and dielectric environment, *J. Phys. Chem. B* 107(3), 668 (2003)
16. J. B. Pendry, L. Martin-Moreno, and F. J. Garcia-Vidal, Mimicking surface plasmons with structured surfaces, *Science* 305(5685), 847 (2004)
17. C. Stampfer, S. Fringes, J. Güttinger, F. Molitor, C. Volk, B. Terrés, J. Dauber, S. Engels, S. Schnez, A. Jacobsen, S. Dröscher, T. Ihn, and K. Ensslin, Transport in graphene nanostructures, *Front. Phys.* 6(3), 271 (2011)
18. K. S. Novoselov, A. K. Geim, S. V. Morozov, D. Jiang, M. I. Katsnelson, I. V. Grigorieva, S. V. Dubonos, and A. A. Firsov, Two-dimensional gas of massless Dirac fermions in graphene, *Nature* 438(7065), 197 (2005)
19. T. Ohta, A. Bostwick, T. Seyller, K. Horn, and E. Rotenberg, Controlling the electronic structure of bilayer graphene, *Science* 313(5789), 951 (2006)
20. M. Orlita, C. Faugeras, P. Plochocka, P. Neugebauer, G. Martinez, D. K. Maude, A.-L. Barra, M. Sprinkle, C. Berger, W. A. de Heer, and M. Potemski, Approaching the Dirac point in high-mobility multilayer epitaxial graphene, *Phys. Rev. Lett.* 101, 267601 (2008)
21. M. Jablan, H. Buljan, and M. Soljacic, Plasmonics in graphene at infrared frequencies, *Phys. Rev. B* 80, 245435 (2009)
22. A. Boltasseva and H. A. Atwater, Low-loss plasmonic metamaterials, *Science* 331(6015), 290 (2011)
23. F. H. L. Koppens, D. E. Chang, and F. J. García de Abajo, Graphene plasmonics: A platform for strong light–matter interactions, *Nano Lett.* 11(8), 3370 (2011)
24. W. Wang, P. Apell, and J. Kinaret, Edge plasmons in graphene nanostructures, *Phys. Rev. B* 84, 085423 (2011)
25. J. Chen, M. Badioli, P. Alonso-Gonzalez, S. Thongrattanasiri, F. Huth, J. Osmond, M. Spasenovic, A. Centeno, A. Pesquera, P. Godignon, A. Z. Elorza, N. Camara, F. J. Garcia de Abajo, R. Hillenbrand, and F. H. Koppens, Optical nano-imaging of gate-tunable graphene plasmons, *Nature* 487, 77 (2012)
26. Z. Fei, A. S. Rodin, G. O. Andreev, W. Bao, A. S. McLeod, M. Wagner, L. M. Zhang, Z. Zhao, M. Thiemens, G.

Dominguez, M. M. Fogler, A. H. Castro Neto, C. N. Lau, F. Keilmann, and D. N. Basov, Gate-tuning of graphene plasmons revealed by infrared nano-imaging, *Nature* 487, 82 (2012)

27. A. Rubio, J. A. Alonso, J. M. Lopez, and M. J. Stott, Surface plasmon excitations in C_{60}, $C_{60}K$ and $C_{60}H$ clusters, *Physica B* 183(3), 247 (1993)
28. J. Yan, Z. Yuan, and S. W. Gao, End and Central plasmon resonances in linear atomic chains, *Phys. Rev. Lett.* 98, 216602 (2007)
29. R. W. Burgess and V. J. Keast, TDDFT study of the optical absorption spectra of bare and coated Au_{55} and Au_{69} clusters, *J. Phys. Chem. C* 115(43), 21016 (2011)
30. H. C. Weissker and C. Mottet, Optical properties of pure and core-shell noble-metal nanoclusters from TDDFT: The influence of the atomic structure, *Phys. Rev. B* 84, 165443 (2011)
31. L. Stella, P. Zhang, F. J. García-Vidal, A. Rubio, and P. García-González, Performance of nonlocal optics when applied to plasmonic nanostructures, *J. Phys. Chem. C* 117(17), 8941 (2013)
32. K. Yabana and G. F. Bertsch, Time-dependent local-density approximation in real time, *Phys. Rev. B* 54(7), 4484 (1996)
33. C. Jamorski, M. E. Casida, and D. R. Salahub, Dynamic polarizabilities and excitation spectra from a molecular implementation of time-dependent density-functional response theory: N_2 as a case study, *J. Chem. Phys.* 104(13), 5134 (1996)
34. J.O. Joswig, L. O. Tunturivuori, and R. M. Nieminen, Photoabsorption in sodium clusters on the basis of time-dependent density-functional theory, *J. Chem. Phys.* 128(1), 014707 (2008)
35. M. A. L. Marques, A. Castro, G. F. Bertsch, and A. Rubio, Octopus: A first-principles tool for excited electron–ion dynamics, *Comput. Phys. Commun.* 151(1), 60 (2003)
36. N. Troullier and J. L. Martins, Efficient pseudopotentials for plane-wave calculations, *Phys. Rev. B* 43(3), 1993 (1991)
37. A. Marinopoulos, L. Reining, V. Olevano, A. Robio, T, Pichler, X. Liu, M. Knupfer, and J. Fink, Anisotropy and interplane interactions in the dielectric response of graphite, *Phys. Rev. Lett.* 89(7): 076402 (2002)
38. F. H. Yin and H. Zhang, Collectivity of plasmon excitations in small sodium clusters with planar structure, *Physica B* 407(3), 416 (2012)